Atmos. Chem. Phys. Discuss., doi:10.5194/acp-2017-222, 2017
Manuscript under review for journal Atmos. Chem. Phys.
Discussion started: 19 April 2017

Atmospheric Chemistry and Physics Discussions

Mixing State of Refractory Black Carbon of the North China Plain Regional Aerosol Combining a Single Particle Soot Photometer and a Volatility Tandem Differential Mobility Analyzer

Yuxuan Zhang[1,2], Hang Su[3,2], Simonas Kecorius[4], Zhibin Wang[4,2], Min Hu[5], Tong Zhu[5], Kebin He[6], Alfred Wiedensohler[4], Qiang Zhang[1] and Yafang Cheng[3,2]

[1]Ministry of Education Key Laboratory for Earth System Modeling, Department of Earth System Science, Tsinghua University, Beijing 100084, China
[2]Multiphase Chemistry Department, Max Planck Institute for Chemistry, Mainz 55020, Germany
[3]Institute for Environmental and Climate Research, Jinan University, Guangzhou 510630, China
[4]Leibniz-Institute for Tropospheric Research, Leipzig 04318, Germany
[5]State Key Joint Laboratory of Environmental Simulation and Pollution Control, College of Environmental Sciences and Engineering, Peking University, Beijing 100871, China
[6]State Key Joint Laboratory of Environment Simulation and Pollution Control, School of Environment, Tsinghua University, Beijing 100084, China

Correspondence to: Yafang Cheng (yafang.cheng@mpic.de) and Hang Su (h.su@mpic.de)

Abstract. Black carbon (BC) aerosol particles play an important role in regulating earth's climate and their climate effects depend on their mixing state. During the CAREBeijing 2013 campaign, we measured the size-resolved mixing state of refractory BC particles in North China Plain and performed intercomparison between a single particle soot photometer (SP2) and a volatility tandem differential mobility analyzer (VTDMA). The intercomparison shows a good agreement between the optical particle diameter determined by SP2 and the mobility particle diameter determined by VTDMA for non-BC as well as for internally mixed refractory BC particles. The VTDMA shows a higher concentration of refractory particles than that of the SP2, which suggests the existence of a large fraction of low volatile non-BC aerosols. Following parameters were constrained by closure studies to improve the inversion of the mixing state of ambient BC (i.e., coating thickness (*CT*) and shell/core ratio (D_p/D_c)) by SP2: a) refractive indices (*RI*) of 1.42 and 1.67-0.56i for non-BC and rBC core components, respectively, b) refractory BC (rBC) core density of 1.2 g cm^{-3} for internally-mixed BC particles, and c) an effective density range of 0.25-0.45 g cm^{-3} for externally-mixed BC particles. Moreover, the upper limit of the measurable particle size of SP2 was extended by the leading-edge-only (LEO) fit from ~400 nm to ~550 nm as confirmed by the VTDMA measurement. Based on the improved inversion from SP2 measurement, we found that non-BC containing particles, internally-mixed BC and externally-mixed BC contribute 85-90%, 5-7% and 5-10% of the total aerosol number in the size range of 200 nm to 350 nm. The number fraction of internally-mixed BC in total BC-containing aerosols (F_{in}) shows pronounced diurnal cycles with a peak around noon time and an apparent turnover rate up to 6-9% h^{-1}. Such diurnal cycles are similar to the finding of Cheng et al. (2012) suggesting the competing effect of emissions and aging processes. In this study, the observed internally-mixed BC particles in the polluted regional NCP (North China Plain) background site (Xianghe) suggest a rapid aging

Atmos. Chem. Phys. Discuss., doi:10.5194/acp-2017-222, 2017
Manuscript under review for journal Atmos. Chem. Phys.
Discussion started: 19 April 2017

Atmospheric Chemistry and Physics Discussions

process of BC on the regional scale. During the intensive field study period, ~80% of internally-mixed BC particles at 200-300 nm showed a D_p/D_c ratio of more than 2, accompanying with an average value of 2.3-2.8. Meanwhile, the *CT* of internally-mixed BC particles (200-350 nm) with rBC core size of 80-200 nm was in the range of 50-150 nm. Compared with previous measurements in developed countries, the observed BC particles on regional scale (i.e., internally-mixed BC particles) were more-aged, indicating stronger optical and climate effect of BC on the regional scale in northern China.

1 Introduction

Black carbon (BC) as a light absorbing aerosol compound have been suggested as the second most important climate-warming agent due to human emissions and plays an important role in the Earth's climate system (Cappa et al., 2012; Cheng et al., 2006; Cheng et al., 2012; Cheng et al., 2008; Fuller et al., 1999;Jacobson, 2001; Japar et al., 1986; Rosen et al., 1978; Rose et al. 2011). It can directly contribute to the particulate matter (PM) pollution (Zheng et al. 2015) or indirectly enhance air pollution by modifying the planetary boundary layer meteorology (Ding et al. 2016). Current uncertainties in assessing the radiative effect of BC may be due to uncertainties in the model treatment of BC emissions, size segregation (Chen et al. 2016; Nordmann et al. 2014) and removal processes as well as the BC mixing state.

The radiative effect of BC strongly depends on its mixing state (how BC is mixed with other aerosol components), of which insufficient knowledge results in largest uncertainties in the estimation of its climate effect (Cappa et al. 2012; Nordmann et al. 2014). Several online techniques have been developed to characterize the mixing state of BC, such as volatility tandem differential mobility analyzer (VTDMA) (Cheng et al., 2012; Philippin et al., 2004; Wehner et al., 2004; Zhang et al, 2016a), single particle soot photometer (SP2) (Metcalf et al., 2013; Schwarz et al., 2006; Sedlacek et al., 2012) and derivative techniques such as soot particle aerosol mass spectrometer (SP-AMS) (Cappa et al., 2012; Lee et al., 2015). This study focuses on the two techniques of VTDMA and SP2. The VTDMA method investigates the mixing state of BC particle by measuring the change of aerosol particle size at different temperatures. As a refractory component, BC will remain in the particle phase upon heating while the rest components tend to evaporate resulting in a change of particle size (Cheng et al., 2009; Frey et al., 2008; Wehner et al., 2009). The change is then used to discriminate internally-mixed BC from externally-mixed ones and to derive the coating thickness. There exist uncertainties in estimate of BC mixing state using VTDMA measurement. The causes are due to that VTDMA cannot identify doubly/multiply charged particles and cannot isolate the influence of low-volatile components (i.e., refractory organic matter (OM), mineral dust, trace metals and/or sea salt) (Cheng et al., 2009).

The SP2 technique characterizes the mixing state of single BC particle through its laser-induced incandescence and scattering properties. The refractory BC (rBC) mass is determined from incandescence intensity and the total particle size is retrieved from its scattering properties. The coating thickness can be calculated from BC mass and the total particle size. The inversion of total particle size, however, is very challenging in early SP2 studies. This is because the initial scattering properties changes with evaporation of coatings for BC-containing particles. The initial scattering properties of BC-

Atmos. Chem. Phys. Discuss., doi:10.5194/acp-2017-222, 2017
Manuscript under review for journal Atmos. Chem. Phys.
Discussion started: 19 April 2017

containing particle are necessary to be inverted for estimating the optical size. To overcome this problem, Gao et al. (2007) developed a leading-edge-only (LEO) fit method to derive the initial scattering properties of aerosol particles, especially BC-containing particles. The SP2 have still limitations in determining the mixing state of BC aerosol. The uncertainties of SP2 technique are mainly due to the uncertainties of the input parameters for the Mie calculation. These input parameters include refractive index (*RI*), the density of BC core, and the morphology of particles (Cappa et al., 2012).

Owing to intensive BC emissions, China has been one of the hot spots of global absorbing aerosol. The amount of BC emissions in China are around 1.8 Tg in the year 2006 estimated by Zhang et al. (2009). BC solar absorption in China plays an important role in global climate change. Model studies show that the BC absorption can be enhanced by a factor of 2-3 as a result of BC mixing with secondary species (Jacobson et al., 2001; Bond et al., 2006; Cheng et al. 2006). Therefore, the BC mixing state in China becomes an important issue in estimate of the regional forcing of BC aerosols. However, to date, there are few reports on BC mixing state (i.e., coating thickness (*CT*) and shell/core ratio (D_p/D_c)) in China due to the limitations in measurement techniques.

In this study, we measured BC mixing state combining SP2 and VTDMA techniques in northern China. Firstly, the single particle size of non-BC, externally-mixed BC and internally-mixed BC measured in SP2 was accurately inverted by parameterization of particle characteristics (i.e., refractive index, effective density and morphology) observed in our site. Compared with SP2 measurement (as a standard reference), we then discussed the performance of VTDMA measurement and potential methods to reduce their uncertainties. Finally, the mixing state of ambient BC aerosols observed in our site were quantified to investigate the BC aging on regional scale of the North China Plain.

2 Methodology

2.1 Experimental setup

As a part of the CAREBeijing 2013 campaign, we performed in site measurements of BC-containing particles from 8 July to 27 July at the regional Atmospheric Observatory Xianghe (39.80°N, 116.96 °E) in the polluted North China Plain. The Xianghe site is located in the southeast of the capital Beijing (~60 km) and northwest of the megacity Tianjin (~100 km), which is surrounded by residential suburban areas and around 5 km from the local town center (Kecorius et al., 2015; Ma et al., 2016; Teich et al. 2016).

The ambient aerosol particles were collected by a sampling system comprised of a PM_{10} cyclone inlet and an automated diffusion dryer (Tuch et al., 2009), and then analyzed by a combination of a SP2 and a VTDMA. A special configuration is that the SP2 was installed after the first differential mobility analyzer (DMA1) of the VTDMA to investigate the ability of SP2 in the inversion of particle sizes (Fig. 1). Since SP2 is recommended for measuring particles with diameters of 200 nm to 400 nm, four sizes (mobility diameter) in this range were selected in our measurements, i.e., 200 nm, 250 nm, 300 nm and 350 nm.

The VTDMA consists of two DMA (labeled as DMA1 and DMA2), two CPC (condensation particle counter) and two

Atmos. Chem. Phys. Discuss., doi:10.5194/acp-2017-222, 2017
Manuscript under review for journal Atmos. Chem. Phys.
Discussion started: 19 April 2017

thermodenuders. DMA1 is used to select mono-dispersed aerosol particles, which are then passed through either a 300 °C thermodenuder or a tube kept at 25°C. The 300 °C thermodenuder is used to remove the volatile components for the determination of nonvolatile/refractory materials. The 25°C tube is used as a reference channel. The number size distribution of residual particles after the thermodnuder is measured by the DMA2 and CPC2. The residual materials after being heated at 300°C were mostly considered as BC components (Cheng et al., 2009; Wehner et al., 2009). Details about the VTDMA system can be found in the work of Philippin et al., 2004; Wehner et al., 2009; and Cheng et al., 2009.

As shown in Fig. 1, we also used a SP2 to measure the mono-dispersed particles selected by DMA1. The mass of rBC can be quantified by its incandescence signals. The SP2 can also determine the optical diameter of single particle from its scattering signals and the goal of performing size-resolved SP2 measurements (DMA1+SP2) is to evaluate its sizing ability. Detailed description of the SP2 instrument could be found in the work of Schwarz et al., 2006; Gysel et al., 2011; Moteki and Kondo, 2007, Zhang et al., 2016b.

2.2 Data analysis

2.2.1 Classification of aerosol particles measured by SP2

In this study, ambient particles are classified into non-BC particles and BC-containing particles (i.e., externally-mixed BC and externally-mixed BC). Particles with detectable amounts of rBC by SP2 are considered as BC-containing particles. According to the lagtimes (Δt), namely the time of the peak of the incandescence signal minus the time of the peak of the scattering signal (Moteki and Kondo, 2007; Schwarz et al., 2006; Sedlacek et al., 2012; Subramanian et al., 2010), BC-containing particles are further classified into externally-mixed BC (Δt <1.6 μs) and internally-mixed BC (Δt >=1.6 μs).

2.2.2 Morphology and effective density of BC

For internally-mixed BC, the rBC core is characterized by a near-spherical shape with an effective density (ρ_{eff}) of 1.2 g m^{-3} as detailed in Zhang et al. (2016b). For externally-mixed BC particle, it is characterized by irregular morphology with smaller effective density (Park et al., 2003; Slowik et al., 2004). The morphology of externally-mixed BC is determined by the relationship between the rBC mass (M) and BC mobility size (D_m) (Park et al., 2003), as in Eq. (1):

$$M = aD_m{}^{D_f}, \quad (1)$$

where the M and D_m were measured by the SP2 and the DMA1 of VTDMA, respectively; a is the parameter of mass-mobility fit; D_f represents fractal dimension of particle, D_f of 3 for spherical particle and 1<D_f<3 for non-spherical particle. The effective density (ρ_{eff}) of externally-mixed BC is also derived by M and D_m (Zhang et al., 2008), expressed by Eq. (2):

$$\rho_{eff} = \frac{6M}{\pi D_m^3}, \quad (2).$$

2.2.3 Optical size derived from SP2

SP2 data have been used to determine the optical particle diameter through their scattering signals. This information is

Atmos. Chem. Phys. Discuss., doi:10.5194/acp-2017-222, 2017
Manuscript under review for journal Atmos. Chem. Phys.
Discussion started: 19 April 2017

Atmospheric Chemistry and Physics Discussions

especially important to determine the coating thickness of internally-mixed BC particles. The size inversion by SP2 is based on the Mie theory.

Equations (3) and (4) list the required input parameters for the Mie model calculation. For non-BC particles, its optical diameter $D_{opt,non\text{-}BC}$ can be determined from its scattering cross section (C_s) and the refractive index ($RI_{non\text{-}BC}$) of non-BC components (Cheng et al., 2009; Cheng et al., 2006). For internally-mixed BC particles, we need additional information of the rBC core, i.e., the volume equivalent spherical diameter of the rBC core (D_c) and its refractive index (RI_c) (Cheng et al., 2009; Cheng et al., 2006).

$$D_{opt,non-BC} \sim (C_s,\ RI_{non-BC}), \quad (3)$$

$$D_{opt,In-BC} \sim (C_s, D_c, RI_{non-BC}, RI_c) \sim (C_s, M, \rho_{eff}, RI_{non-BC}, RI_c), \quad (4)$$

In this study, C_s was determined by the LEO fit (Gao et al., 2007). $RI_{non\text{-}BC}$ was determined through a closure study: we scanned different values of $RI_{non\text{-}BC}$ until the calculated optical diameter matches the measured mobility diameter. Figure 2 shows the $RI_{non\text{-}BC}$ determined for non-BC particles. Since a DMA selects only quasi-monodispersed aerosol particles (due to the width of the transfer function), the real diameter shows a distribution rather than a single value of the nominal mobility diameter, which results in a more widely distributed $RI_{non\text{-}BC}$ (~1.2-1.6). To account for this effect, we took only the averaged peak value of each distribution for further calculations, which corresponds to the peak of the DMA transfer function. During the intensive study period, $RI_{non\text{-}BC}$ inversed from different sizes are quite similar with an average of 1.4209. For the validation, we also applied this method to polystyrene latex (PSL) spheres. As shown in Fig. 2, the inversion gives a peak *RI* of 1.5861, the same as the *RI* of PSL (1.59) in literature (Gao et al., 2007).

In Eq. (4), D_c is calculated from its mass (M) and effective density (ρ_{eff}, 1.2 g m^{-3}, Zhang et al. 2016b), as shown in Eq. (5):

$$D_c = \left(\frac{6m}{\pi \rho_{eff}}\right)^{\frac{1}{3}}, \quad (5).$$

For RI_c, we assume that BC and some non-BC materials together make a spherical core and serves as bones and flesh, respectively. Then RI_c can be approximated by the volume-weighted *RI* of the BC and non-BC mixtures as in Eq. (6):

$$RI_c = [n_{BC} \times (1 - R_{void}) + n_{nonBC} \times R_{void}] + [k_{BC} \times (1 - R_{void})]i, \quad (6)$$

In which, n_{BC} and n_{nonBC} are the real parts of *RI* for the BC materials and non-BC components (n_{BC} = 1.95 and n_{nonBC} = 1.42); k_{BC} is the imaginary part of the refractive index for BC (k_{BC} = 0.79) (Bond and Bergstrom, 2006); R_{void} is the volume fraction of internal voids in BC core, which is 0.30 during the campaign based on SP2 and VTDMA measurement (Zhang et al. 2016b).

2.2.4 Mixing state of BC-containing particles

In this study, the mixing state of BC-containing particles is characterized by the coating thickness (*CT*) and the shell/core ratio (D_p/D_c), which can be determined by the whole particle size (D_p) and the rBC core size (D_c), as in Eqs. (7) and (8):

Atmos. Chem. Phys. Discuss., doi:10.5194/acp-2017-222, 2017
Manuscript under review for journal Atmos. Chem. Phys.
Discussion started: 19 April 2017

Atmospheric Chemistry and Physics Discussions

$$\mathrm{CT} = \frac{D_p - D_c}{2}, \quad (7)$$

$$\frac{\text{shell}}{\text{core}} = \frac{D_p}{D_c}, \quad (8).$$

3 Results and discussion

3.1 Particle size derived from SP2 measurement

3.1.1 Non-BC and internally-mixed BC particles

In SP2 measurement, the uncertainties of BC mixing state is mainly from the inversion of particle size. For non-BC and internally-mixed BC particles, their optical size was determined by LEO fit and Mie mode calculation, which was improved by constraining some input parameters (ρ_{eff}, $RI_{\text{non-BC}}$ and RI_{c}, discussed in Sect. 2.2.3). These parameters can reflect the real characteristics of the observed particles at our site.

To evaluate the particle size derived from SP2 measurement, we compared the optical diameter (determined by the SP2) for non-BC and internally-mixed BC particles with the mobility diameter (determined by the DMA1), shown in Fig. 3. The combination of DMA with SP2 makes it possible to distinguish singly charged particles from the doubly/multiply charged particles. Here, we compared the optical diameter of doubly/multiply charged particles with the nominal sizes of those particles in Fig. 3. The optical particle diameter showed an excellent agreement with the mobility diameter, with a difference of ~1%. The agreement revealed that the LEO method was applicable for ambient aerosol particles. It also validated the assumption on a spherical BC particle in the Mie model calculation. The accurate inversion of particle size of internally-mixed BC particles indicated a reliable estimate of their mixing state in this work.

3.1.2 Sizing of externally-mixed BC

For externally-mixed BC particles, a diameter is hard to define due to their irregular morphology (Park et al., 2003; Slowik et al., 2004). Figure 4 shows the fractal dimension and effective density of externally-mixed BC particles observed during the campaign period. The mass-mobility relationship exhibited a power law with a scaling exponent of ~2.23 for externally-mixed BC over the range mobility size from 200 to 350nm, suggesting a fractal dimension of 2.23. Compared with spherical particles (D_{f} of 3), the lower fractal dimension of observed externally-mixed BC particles demonstrated their irregular shape. This indicated that the assumption on a spherical particle in the Mie model was inappropriate for externally-mixed BC particles. Therefore, we did not used the LEO fit and Mie model to calculate the optical size of externally-mixed BC particles based on SP2 measurement in this study.

Figure 5 shows a comparison between its volume equivalent diameter (D_{ve}) and the mobility diameter (D_{m}). The D_{ve} is calculated from its mass and the void-free BC density of 1.8 g m^{-3} (Metcalf et al., 2012; Schwarz et al., 2008; Subramanian et al., 2010). As shown in Fig. 4, the peak in the volume equivalent size distribution of externally-mixed BC were ~120-160

nm, remarkably lower than the mobility size (200-350 nm). The large discrepancy between D_{ve} and D_m suggested that the externally-mixed BC was not a void-free sphere because the internal voids and irregular shape resulted in lower density and larger sized, as observed by DMA. Therefore, it is inappropriate for SP2 measurement using void-free BC density of 1.8 g m^{-3} to calculate the size of externally-mixed BC. In this study, we assumed that there was little coatings on the surface of externally-mixed BC particle, and then used an effective density of 0.25-0.45 g cm^{-3} for externally-mixed BC particle (Fig. 4) to calculate its size based on SP2-measured rBC mass.

3.1.3 The size distribution of charged particles

To further assess the ambient particle size derived from SP2 measurement in our study, we discussed the number size distribution of charged particles (i.e., singly, doubly or triply charged aerosol particles). Our setup (combination of DMA with SP2) is able to separate aerosol particles with different charges. As shown in Fig. 6 (A), the total particle number size distribution is calculated as the sum of optical particle number size distribution of non-BC particles and internally-mixed BC particles, plus the mobility particle number size distribution of externally-mixed BC particle. The first peak of the number size distribution represents the mode of singly charged particles, of which the diameter coincides with the mobility diameter of DMA1 (200, 250, 300 and 350 nm). The second or the third peak corresponds to the mode of doubly or triply charged aerosol particles. We also calculated the theoretical mobility diameter of doubly/triply charged particles. Most of theoretically calculated diameter of double charged or triple charged aerosols agrees well with the measured diameter (323, 414, 438 and 508 nm) except for the double charged particles with a diameter of 601 nm. The result revealed that the LEO fit used in our study was valid for particles with diameters lower than ~550 nm, indicating that our method used in this study extended the measurable size range of SP2 (~200-400 nm).

According to the particle number size distribution shown in Fig. 6 (A), we further calculated the ratio of number concentration between single and double charged particles ($R_{single\text{-}double}$), which was then compared with the theoretical calculated $R_{single\text{-}double}$ values to further assess the optical particle diameter information derived from SP2 measurement. The observed $R_{single\text{-}double}$ was determined by separately integrating the front two peak areas of number size distribution for size-resolved ambient particles while the theoretical calculated $R_{single\text{-}double}$ was derived from bipolar charged distribution (Wiedensohler, 1988; Wiedensohler et al., 2012) and particle number size distribution of ambient particles from mobility particle size spectrometer measurements. As shown in Fig.6 (B), the measured $R_{single\text{-}double}$ showed a good agreement with the theoretically calculated $R_{single\text{-}double}$ with a slope of 0.9090 and a R^2 of 0.9335, which demonstrated the potential of optical sizing instruments (e.g., SP2) in determining the bipolar charge distribution of aerosol particles. Our results further revealed that the accurate particle size was derived by our method (discussed in Sect. 3.3.1 and Sect. 3.3.2) based on SP2 measurement.

3.2 Comparison between SP2 and VTDMA measurements

As SP2 technique, VTDMA measurement can also derive the mixing state of BC-containing particles based on their size

information. BC-containing particles can be determined by SP2 according to the incandescence light emitted at rBC vaporization temperature of ~4000 K. It is also suggested that nonvolatile materials at high temperature determined by VTDMA and other thermodenuder measurements can be considered as BC (Cappa et al. 2012; Cheng et al., 2009; Wehner et al., 2009). In this work, we compared the results of these two methods, i.e., the size distribution of rBC (externally mixed BC and BC core of internally mixed BC) measured by SP2 and that of residual materials from our VTDMA measurement at 300 ºC (Fig. 7). Note that the SP2 detection efficiency and experimentally determined effective density have been considered in the calculation of the rBC size distribution (Fig. S1, S2).

As shown in Fig. 7, the number size distribution exhibited a large discrepancy between the SP2 and VTDMA measurements. The SP2 measurement show two peaks of rBC around prescribed size (200, 250, 300 and 350 nm selected by DMA1) and smaller size, representing externally-mixed BC and internally-mixed BC cores, respectively. For VTDMA measurement, the number size distribution of residual low-volatile particles (300 ºC) also showed a peak of externally-mixed BC, but two peaks at smaller sizes similar to previous measurements in Beijing (Cheng et al., 2012). The discrepancy of size distribution would lead to significant difference in BC mixing state between the SP2 and VTDMA measurements. As our discussed in Sect. 3.1, data inversion of SP2 measurement was accurate in this work, suggesting that VTDMA measurement had a larger uncertainty.

Figure 7 also shows that the VTDMA-produced number concentration of residual aerosol particles at 300 ºC was much higher than the SP2-produced number concentration of rBC. However, the number concentration of the total ambient samples at 200-350 nm (selected by DMA1) measured by SP2 showed an excellent agreement with that measured by VTDMA (counted by CPC1), shown in Fig.S3. If we consider the SP2 results as a standard reference, the higher concentration of VTDMA shown in Fig.7 suggested that there were a large fraction of non-BC aerosol particles which contained low-volatile components (e.g. refractory OM, mineral dust, trace metals and sea salt) (Cheng et al., 2009; Ehn et al., 2014; Kalberer et al., 2004). The number concentration of rBC particles from SP2 measurement accounted for ~20% of residual particles measured by VTDMA. During the intensive study period, lots of non-BC particles that could not completely volatile at 300°C and just shrank to smaller particles, would cause uncertainties of BC mixing state estimated by VTDMA measurement. To improve VTDMA measurement, it is important to quantify low-volatile components.

3.3 BC mixing state

As discussed above, more accurate size information obtained by SP2 measurement in this work can improve the estimate of mixing state for ambient BC-containing particles. The BC mixing state observed at our site (i.e., Xianghe), especially for internally-mixed BC particles, can characterize the BC aging process during regional transport, considering that Xianghe is a polluted regional background site of the North China Plain influenced by mixed regional emission sources from the Jing-Jin-Ji region.

During the campaign period, the size-resolved number and mass fraction of BC and non-BC are shown in Fig.8. Most of ambient aerosol particles are non-BC particles in the investigated size range (200 nm to 350 nm) while the BC-containing

Atmos. Chem. Phys. Discuss., doi:10.5194/acp-2017-222, 2017
Manuscript under review for journal Atmos. Chem. Phys.
Discussion started: 19 April 2017

Atmospheric Chemistry and Physics Discussions

particles contribute a number fraction of 7-10% (Fig. 8A). Concerning the mass fraction, the BC components (externally-mixed BC and internally-mixed BC core) account for 3-7% of the particle mass in the investigated size range (200 nm to 350nm) while the non-BC component (including non-BC particles and internally-mixed BC shell) contributes more than 90% of particle mass (Fig. 8B), which was consist with previous studies in Jing-Jin-Ji region (Yang et al., 2015; Zheng et al., 2015). The smaller contribution of BC as a primary component, revealed that the aerosol particles sampled at our site was mostly from regional sources and likely underwent a long-range transport. When long-range transport was a dominant influence, the BC-containing particles would be more-aged. Figure 8B shows that the mass of the BC shell for internally-mixed BC particles was about 3 times higher than that of the BC core, suggesting the nature of thick coating.

For internally-mixed BC particles observed in our site, their mixing state reflected the long-range transport of aged aerosol from regional sources of the North China Plain. During the intensive study period, the fraction of internally-mixed BC particles ($F_{\text{In-BC}}$) at 200-300 nm were 38-51% (Fig. 8A). The $F_{\text{In-BC}}$ showed pronounce diurnal variation, with a maximum at~14:00 LT and a minimum at morning rush hours (~07:00 LT) (Fig. 9). The peak around noontime can be attributed to secondary photochemical formation and regional transport. On the other hand, the low $F_{\text{In-BC}}$ in the morning rush hours was due to the large contribution of fresh BC particles from traffic emissions. F_{in} then increased from 8:00 to 14:00, with an apparent turnover rate up to 6-9% h^{-1} for BC-containing particles at 200-350 nm, which was consistent with the finding of Cheng et al. (2012). The results suggested the observed mixing state of BC-containing particles were subject to the competing effect of emissions and aging processes. To investigate the BC aging on regional scale, we quantified the mixing state of internally-mixed BC particles (i.e., *CT* and D_p/D_c ratio) observed at our site in the following analysis.

Figure 10 shows that the relative contribution of different D_p/D_c ratio of internally-mixed BC particles at 200-350 nm. The observed internally-mixed BC aerosols are dominated by particles with D_p/D_c ratio of 2-3, ~80% of internally-mixed BC particles with a D_p/D_c ratio more than 2. On average, the D_p/D_c ratio of internally-mixed BC particles at 200-350 nm were 2.3-2.7, which increased as the particle size increases. The results revealed that BC was fully aged during regional transport from the Jing-Jin-Ji region in the North China Plain, which can be attributed to large-scale regional production by secondary process in the atmosphere (e.g., oxidation of SO_2, NO_x and volatile organic carbon (VOC) to sulfate, nitrate and secondary organic aerosol (SOA), respectively) (Andreae et al., 2008). The thick coatings on the surface of internally-mixed BC observed at Xianghe site suggested that the absorption of BC from regional sources in the North China Plain could be strongly enhanced by the lensing effect of coatings (Zhang et al., 2016b).

According to the diffusion-controlled growth law of BC aging during the atmospheric process (Seinfeld and Pandis, 2006), the amount of coating materials on BC surface is size-dependent. Figure 11 shows the coating thickness of internally-mixed BC particles as a function of rBC core size (D_c). The *CT* of internally-mixed BC particles decreased as D_c increased and increased as the BC particle size (D_p) increased, following the diffusion-controlled growth law. For internally-mixed BC particles of 200-350 nm, the D_c and *CT* showed a wide mode, which were in the range of ~80-200 nm and ~50-150 nm, respective. The wide range of D_c and *CT* revealed that the internally-mixed BC particles at our site consisted of a mixture of BC from various regional sources of the North China Plain. The more-aged BC particles were mostly from long-range

Atmos. Chem. Phys. Discuss., doi:10.5194/acp-2017-222, 2017
Manuscript under review for journal Atmos. Chem. Phys.
Discussion started: 19 April 2017

transport from polluted regions (i.e., the densely populated and industrialized regions such as the megacities Beijing and Tianjin).

In this work, we found that the BC aerosols of the North China Plain were more-aged than BC aerosols observed in those observed in developed countries (Table 1). The thicker coating suggests a faster aging rate of BC aerosols in the North China Plain, which can be attributed to much higher concentration of aerosols and condensable vapors in China compared to those in developed countries. The more-aged BC aerosols in China could lead to stronger absorptivity of BC, suggesting the important contribution of BC aerosols in China to climate change.

4 Conclusions

The light absorption of BC-containing particles strongly depends on their mixing state. In this work, we have investigated the comprehensive characterization of BC mixing state at a polluted regional background site (Xianghe) of the North China Plain during the summer of 2013. Our work provides the information on ambient BC aging in northern China based on in situ measurement.

In this study, the mixing state of BC-containing particles (i.e., *CT* and D_p/D_c ratio) was determined by the BC size. In SP2 measurement, the optical sizes of non-BC particles and internally-mixed BC particles were calculated by LEO fit and Mie mode, which was improved with more accurate input parameters ($RI_{non\text{-}BC}$=1.42, RI_c=1.67-0.56i, ρ_c=1.2 g cm^{-3}). However, the size of an externally-mixed BC particle measured by SP2 was characterized by mobility size according to its mass and effective density (0.25-0.45 g cm^{-3}) due to its irregular shape (fractal dimension of 2.23). Using our method to inverse particle size, the upper limit of the measurable particle size of SP2 was extended from ~400 nm to ~550 nm as confirmed by the VDMA measurement. The particle size derived from SP2 in this work have been demonstrated to be accurate for estimate of BC mixing state.

Considering the SP2 results as a standard reference, we found that low-volatile non-BC materials at 300 ºC would affect the estimate of BC mixing state by VTDMA measurement. During the campaign at our site, about ~80% of remained particles in number concentration after 300 ºC were low-volatile non-BC particles. In this case, the mixing state of ambient BC determining by VTDMA existed a large uncertainty. To improve VTDMA measurement, quantifying the low-volatile non-BC materials should be conducted, which will be discussed in our future study.

We quantified BC mixing state during an intensive field campaign in North China using the SP2 results. The BC-containing particles account for 7-10% of the particle number in the investigated size range (200 nm to 350nm), while the externally-mixed BC, internally-mixed BC core and coating components contributed 2-3%, 1-4% and 7-10% of particle mass, respectively. Larger particles tended to have more internally-mixed BC particles and BC coating materials. The component analysis indicated that the aerosol particles observed at our site was mostly from regional sources.

The internally-mixed BC particles at the polluted regional background site (Xianghe) could characterize the BC mixing state on regional scale (i.e., Jing-Jin-Ji region). During the campaign period, the $F_{In\text{-}BC}$ was 38-51% for BC-containing

particles of 200-350 nm, with an apparent turnover rate up to 6-9% h^{-1} at noon time, indicating a rapid aging process of BC on the regional scale. The average D_p/D_c of internally-mixed BC particles at 200-350 nm was 2.3-2.7, while the number fraction of D_p/D_c more than 2 was ~80%, indicated that the observed BC-containing particles from regional sources of the North China Plain were strongly aged during regional transport. The internally-mixed BC particles at 200-350 nm showed a rBC core size in the range of ~80-200 nm, accompanying with *CT* of ~50-150 nm. The wide range of rBC size and *CT* revealed the BC aerosols observed in our site from various regional sources. More-aged BC particles on regional scale was found in China compared with those observed in developed countries, indicating stronger light absorptivity of BC. Our results suggested the importance of BC aerosols in polluted regions (e.g., Jing-Jin-Ji region) in China to climate change.

Acknowledgments

This work was funded by the National Natural Science Foundation of China (41571130035, 41625020, 41330635, 21107061, and 21190054), the Max Planck Society (MPG) Minerva program and the EU project BACCHUS (603445).

References

Andreae, M. O., Schmid, O., Yang, H., Chand, D., Zhen Yu, J., Zeng, L.-M., and Zhang, Y.-H.: Optical properties and chemical composition of the atmospheric aerosol in urban Guangzhou, China, *Atmos. Environ.*, 42, 6335-6350, 2008.

Bond, T. C., and Bergstrom R. W.: Light Absorption by Carbonaceous Particles: An Investigative Review, *Aerosol Sci. Technol.*, 40, 27-67, 2006.

Cappa, C. D., Onasch, T. B., Massoli, P., Worsnop, D. R., Bates, T. S., Cross, E. S., Davidovits, P., Hakala, J., Hayden, K. L., Jobson, B. T., Kolesar, K. R., Lack, D. A., Lerner, B. M., Li, S.-M., Mellon, D., Nuaaman, I., Olfert, J. S., Petäjä, T., Quinn, P. K., Song, C., Subramanian, R., Williams, E. J., and Zaveri, R. A.: Radiative Absorption Enhancements Due to the Mixing State of Atmospheric Black Carbon, *Science*, 337, 1078-1081, 2012.

Chen, Y., Cheng, Y. F., Nordmann, S., Birmili, W., Denier van der Gon, H. A. C., Ma, N., Wolke, R., Wehner, B., Sun, J., Spindler, G., Mu, Q., Pöschl, U., Su, H., and Wiedensohler, A.: Evaluation of the size segregation of elemental carbon (EC) emission in Europe: influence on the simulation of EC long-range transportation, *Atmos. Chem. Phys.*, 16, 1823-1835, 2016.

Cheng, Y. F., Eichler, H., Wiedensohler, A., Heintzenberg, J., Zhang, Y. H., Hu, M., Herrmann, H., Zeng, L. M., Liu, S., Gnauk, T., Brüggemann, E., and He, L. Y.: Mixing state of elemental carbon and non-light-absorbing aerosol components derived from in situ particle optical properties at Xinken in Pearl River Delta of China, *J. Geophys. Res.-Atmos.*, 111, 2006.

Cheng, Y. F., Wiedensohler, A., Eichler, H., Su, H., Gnauk, T., Brüggemann, E., Herrmann, H., Heintzenberg, J., Slanina, J., Tuch, T., Hu, M., and Zhang, Y. H.: Aerosol optical properties and related chemical apportionment at Xinken in Pearl River Delta of China, *Atmos. Environ.*, 42, 6351-6372, 2008.

Cheng, Y. F., Berghof, M., Garland, R. M., Wiedensohler, A., Wehner, B., Müller, T., Su, H., Zhang, Y. H., Achtert, P.,

Nowak, A., Pöschl, U., Zhu, T., Hu, M., and Zeng, L. M.: Influence of soot mixing state on aerosol light absorption and single scattering albedo during air mass aging at a polluted regional site in northeastern China, *J. Geophys. Res.-Atmos.*, 2009.

Cheng, Y. F., Su, H., Rose, D., Gunthe, S. S., Berghof, M., Wehner, B., Achtert, P., Nowak, A., Takegawa, N., Kondo, Y., Shiraiwa, M., Gong, Y. G., Shao, M., Hu, M., Zhu, T., Zhang, Y. H., Carmichael, G. R., Wiedensohler, A., Andreae, M. O., and Pöschl, U.: Size-resolved measurement of the mixing state of soot in the megacity Beijing, China: diurnal cycle, aging and parameterization, *Atmos. Chem. Phys.*, 12, 4477-4491, 2012.

Ding, A. J., Huang, X., Nie, W., Sun, J. N., Kerminen, V. M., Petäjä, T., Su, H., Cheng, Y. F., Yang, X. Q., Wang, M. H., Chi, X. G., Wang, J. P., Virkkula, A., Guo, W. D., Yuan, J., Wang, S. Y., Zhang, R. J., Wu, Y. F., Song, Y., Zhu, T., Zilitinkevich, S., Kulmala, M., and Fu, C. B.: Enhanced haze pollution by black carbon in megacities in China, *Geophys. Res. Lett.*, 2016.

Ehn, M., Thornton, J. A., Kleist, E., Sipila, M., Junninen, H., Pullinen, I., Springer, M., Rubach, F., Tillmann, R., Lee, B., Lopez-Hilfiker, F., Andres, S., Acir, I.-H., Rissanen, M., Jokinen, T., Schobesberger, S., Kangasluoma, J., Kontkanen, J., Nieminen, T., Kurten, T., Nielsen, L. B., Jorgensen, S., Kjaergaard, H. G., Canagaratna, M., Maso, M. D., Berndt, T., Petaja, T., Wahner, A., Kerminen, V.-M., Kulmala, M., Worsnop, D. R., Wildt, J., and Mentel, T. F.: A large source of low-volatility secondary organic aerosol, *Nature*, 506, 476-479, 2014.

Frey, A., Rose, D., Wehner, B., Müller, T., Cheng, Y., Wiedensohler, A., and Virkkula, A.: Application of the Volatility-TDMA Technique to Determine the Number Size Distribution and Mass Concentration of Less Volatile Particles, *Aerosol Sci. Technol.*, 42, 817-828, 2008.

Fuller, K. A., Malm, W. C., and Kreidenweis, S. M.: Effects of mixing on extinction by carbonaceous particles, *J. Geophys. Res.-Atmos.*, 104, 15941-15954, 1999.

Gao, R. S., Schwarz, J. P., Kelly, K. K., Fahey, D. W., Watts, L. A., Thompson, T. L., Spackman, J. R., Slowik, J. G., Cross, E. S., Han, J. H., Davidovits, P., Onasch, T. B., and Worsnop, D. R.: A Novel Method for Estimating Light-Scattering Properties of Soot Aerosols Using a Modified Single-Particle Soot Photometer, *Aerosol Sci. Technol.*, 41, 125-135, 2007.

Gysel, M., Laborde, M., Olfert, J. S., Subramanian, R., and Gröhn, A. J.: Effective density of Aquadag and fullerene soot black carbon reference materials used for SP2 calibration, *Atmos. Meas. Tech.*, 4, 2851-2858, 2011.

Jacobson, M. Z.: Strong radiative heating due to the mixing state of black carbon in atmospheric aerosols, *Nature*, 409, 695-697, 2001.

Japar, S. M., Brachaczek, W. W., Gorse Jr, R. A., Norbeck, J. M., and Pierson, W. R.: The contribution of elemental carbon to the optical properties of rural atmospheric aerosols, *Atmos. Environ.*, 20, 1281-1289, 1986.

Kalberer, M., Paulsen, D., Sax, M., Steinbacher, M., Dommen, J., Prevot, A. S. H., Fisseha, R., Weingartner, E., Frankevich, V., Zenobi, R., and Baltensperger, U.: Identification of Polymers as Major Components of Atmospheric Organic Aerosols, *Science*, 303, 1659-1662, 2004.

Kecorius, S., Zhang, S., Wang, Z., Gross, J., Ma, N., Wu, Z., Ran, L., Hu, M., Wang, P., Ulevicius, V., and Wiedensohler, A.: Nocturnal Aerosol Particle Formation in the North China Plain, *Lith. J. Phys.*, 55, 44-53, 2015.

Laborde, M., Crippa, M., Tritscher, T., Jurányi, Z., Decarlo, P. F., Temime-Roussel, B., Marchand, N., Eckhardt, S., Stohl, A., Baltensperger, U., Prévôt, A. S. H., Weingartner, E., and Gysel, M.: Black carbon physical properties and mixing state in the European megacity Paris, *Atmos. Chem. Phys.*, 13, 5831-5856, 2013.

Lee, A. K. Y., Willis, M. D., Healy, R. M., Onasch, T. B., and Abbatt, J. P. D.: Mixing state of carbonaceous aerosol in an urban environment: single particle characterization using the soot particle aerosol mass spectrometer (SP-AMS), *Atmos. Chem. Phys.*, 15, 1823-1841, 2015.

Ma, N., Zhao, C., Tao, J., Wu, Z., Kecorius, S., Wang, Z., Größ, J., Liu, H., Bian, Y., Kuang, Y., Teich, M., Spindler, G., Müller, K., van Pinxteren, D., Herrmann, H., Hu, M., and Wiedensohler, A.: Variation of CCN activity during new particle formation events in the North China Plain, *Atmos. Chem. Phys.*, 16, 8593-8607, 2016.

Metcalf, A. R., Craven, J. S., Ensberg, J. J., Brioude, J., Angevine, W., Sorooshian, A., Duong, H. T., Jonsson, H. H., Flagan, R. C., and Seinfeld, J. H.: Black carbon aerosol over the Los Angeles Basin during CalNex, *J. Geophys. Res.-Atmos.*, 117, 2012.

Metcalf, A. R., Loza, C. L., Coggon, M. M., Craven, J. S., Jonsson, H. H., Flagan, R. C., and Seinfeld, J. H.: Secondary Organic Aerosol Coating Formation and Evaporation: Chamber Studies Using Black Carbon Seed Aerosol and the Single-Particle Soot Photometer, *Aerosol Sci. Technol*., 47, 326-347, 2013.

Moteki, N., and Kondo, Y.: Effects of Mixing State on Black Carbon Measurements by Laser-Induced Incandescence, *Aerosol Sci. Technol.*, 41, 398-417, 2007.

Nordmann, S., Cheng, Y. F., Carmichael, G. R., Yu, M., Denier van der Gon, H. A. C., Zhang, Q., Saide, P. E., Pöschl, U., Su, H., Birmili, W., and Wiedensohler, A.: Atmospheric black carbon and warming effects influenced by the source and absorption enhancement in central Europe, *Atmos. Chem. Phys.*, 14, 12683-12699, 2014.

Park, K., Cao, F., Kittelson, D. B., and McMurry, P. H.: Relationship between Particle Mass and Mobility for Diesel Exhaust Particles, *Environ. Sci. Technol.*, 37, 577-583, 2003.

Philippin, S., Wiedensohler, A., and Stratmann, F.: Measurements of non-volatile fractions of pollution aerosols with an eight-tube volatility tandem differential mobility analyzer (VTDMA-8), *J. Aerosol Sci.,* 35, 185-203, 2004.

Rose, D., Gunthe, S. S., Su, H., Garland, R. M., Yang, H., Berghof, M., Cheng, Y. F., Wehner, B., Achtert, P., Nowak, A., Wiedensohler, A., Takegawa, N., Kondo, Y., Hu, M., Zhang, Y., Andreae, M. O., and Pöschl, U.: Cloud condensation nuclei in polluted air and biomass burning smoke near the mega-city Guangzhou, China-Part 2: Size-resolved aerosol chemical composition, diurnal cycles, and externally mixed weakly CCN-active soot particles, *Atmos. Chem. Phys.*, 11, 2817-2836, 2011.

Rosen, H., Hansen, A. D. A., Gundel, L., and Novakov, T.: Identification of the optically absorbing component in urban aerosols, *Appl. Opt.*, 17, 3859-3861, 1978.

Schwarz, J. P., Gao, R. S., Fahey, D. W., Thomson, D. S., Watts, L. A., Wilson, J. C., Reeves, J. M., Darbeheshti, M., Baumgardner, D. G., Kok, G. L., Chung, S. H., Schulz, M., Hendricks, J., Lauer, A., Kärcher, B., Slowik, J. G., Rosenlof, K. H., Thompson, T. L., Langford, A. O., Loewenstein, M., and Aikin, K. C.: Single-particle measurements of midlatitude black

carbon and light-scattering aerosols from the boundary layer to the lower stratosphere, *J. Geophys. Res.-Atmos.*, 111, 2006.

Schwarz, J. P., Gao, R. S., Spackman, J. R., Watts, L. A., Thomson, D. S., Fahey, D. W., Ryerson, T. B., Peischl, J., Holloway, J. S., Trainer, M., Frost, G. J., Baynard, T., Lack, D. A., de Gouw, J. A., Warneke, C., and Del Negro, L. A.: Measurement of the mixing state, mass, and optical size of individual black carbon particles in urban and biomass burning emissions, *Geophys. Res. Lett.*, 35, 2008.

Sedlacek, A. J., Lewis, E. R., Kleinman, L., Xu, J., and Zhang, Q.: Determination of and evidence for non-core-shell structure of particles containing black carbon using the Single-Particle Soot Photometer (SP2), *Geophys. Res. Lett.*, 39, 2012.

Seinfeld, J. H., and Pandis, S. N.: Atmospheric Chemistry and Physics: From Air Pollution to Climate Change, 2nd ed. *John Wiley & Sons, Inc*., New York, 2006.

Shiraiwa, M., Kondo, Y., Moteki, N., Takegawa, N., Sahu, L. K., Takami, A., Hatakeyama, S., Yonemura, S., and Blake, D. R.: Radiative impact of mixing state of black carbon aerosol in Asian outflow, *J. Geophys. Res.-Atmos.*, 2008.

Slowik, J. G., Stainken, K., Davidovits, P., Williams, L. R., Jayne, J. T., Kolb, C. E., Worsnop, D. R., Rudich, Y., DeCarlo, P. F., and Jimenez, J. L.: Particle Morphology and Density Characterization by Combined Mobility and Aerodynamic Diameter Measurements. Part 2: Application to Combustion-Generated Soot Aerosols as a Function of Fuel Equivalence Ratio, *Aerosol Sci. Technol.*, 38, 1206-1222, 2004.

Subramanian, R., Kok, G. L., Baumgardner, D., Clarke, A., Shinozuka, Y., Campos, T. L., Heizer, C. G., Stephens, B. B., de Foy, B., Voss, P. B., and Zaveri, R. A.: Black carbon over Mexico: the effect of atmospheric transport on mixing state, mass absorption cross-section, and BC/CO ratios, *Atmos. Chem. Phys.*, 10, 219-237, 2010.

Taylor, J. W., Allan, J. D., Liu, D., Flynn, M., Weber, R., Zhang, X., Lefer, B. L., Grossberg, N., Flynn, J., and Coe, H.: Assessment of the sensitivity of core / shell parameters derived using the single-particle soot photometer to density and refractive index, *Atmos. Meas. Tech*., 8, 1701-1718, 2015.

Teich, M., van Pinxteren, D., Kecorius, S., Wang, Z., and Herrmann, H.: First Quantification of Imidazoles in Ambient Aerosol Particles: Potential Photosensitizers, Brown Carbon Constituents, and Hazardous Components, *Environ. Sci. Technol.*, 50, 1166-1173, 2016.

Tuch, T. M., Haudek, A., Müller, T., Nowak, A., Wex, H., and Wiedensohler, A.: Design and performance of an automatic regenerating adsorption aerosol dryer for continuous operation at monitoring sites, *Atmos. Meas. Tech.*, 2, 417-422, 2009.

Wehner, B., Philippin, S., Wiedensohler, A., Scheer, V., and Vogt, R.: Variability of non-volatile fractions of atmospheric aerosol particles with traffic influence, *Atmos. Environ.*, 38, 6081-6090, 2004.

Wehner, B., Berghof, M., Cheng, Y. F., Achtert, P., Birmili, W., Nowak, A., Wiedensohler, A., Garland, R. M., Pöschl, U., Hu, M., and Zhu, T.: Mixing state of nonvolatile aerosol particle fractions and comparison with light absorption in the polluted Beijing region, *J. Geophys. Res.-Atmos.*, 114, 2009.

Wiedensohler, A.: An approximation of the bipolar charge distribution for particles in the submicron size range, *J. Aerosol Sci.,* 19, 387-389, 1988.

Wiedensohler, A., Birmili, W., Nowak, A., Sonntag, A., Weinhold, K., Merkel, M., Wehner, B., Tuch, T., Pfeifer, S., Fiebig,

M., Fjäraa, A. M., Asmi, E., Sellegri, K., Depuy, R., Venzac, H., Villani, P., Laj, P., Aalto, P., Ogren, J. A., Swietlicki, E., Williams, P., Roldin, P., Quincey, P., Hüglin, C., Fierz-Schmidhauser, R., Gysel, M., Weingartner, E., Riccobono, F., Santos, S., Grüning, C., Faloon, K., Beddows, D., Harrison, R., Monahan, C., Jennings, S. G., O'Dowd, C. D., Marinoni, A., Horn, H. G., Keck, L., Jiang, J., Scheckman, J., McMurry, P. H., Deng, Z., Zhao, C. S., Moerman, M., Henzing, B., de Leeuw, G., Löschau, G., and Bastian, S.: Mobility particle size spectrometers: harmonization of technical standards and data structure to facilitate high quality long-term observations of atmospheric particle number size distributions, *Atmos. Meas. Tech.*, 5, 657-685, 2012.

Yang, Y. R., Liu, X. G., Qu, Y., An, J. L., Jiang, R., Zhang, Y. H., Sun, Y. L., Wu, Z. J., Zhang, F., Xu, W. Q., and Ma, Q. X.: Characteristics and formation mechanism of continuous hazes in China: a case study during the autumn of 2014 in the North China Plain, *Atmos. Chem. Phys.*, 15, 2015.

Zhang, Q., Streets, D. G., Carmichael, G. R., He, K. B., Huo, H., Kannari, A., Klimont, Z., Park, I. S., Reddy, S., Fu, J. S., Chen, D., Duan, L., Lei, Y., Wang, L. T., and Yao, Z. L.: Asian emissions in 2006 for the NASA INTEX-B mission, *Atmos. Chem. Phys.*, 9, 5131-5153, 2009.

Zhang, R., Khalizov, A. F., Pagels, J., Zhang, D., Xue, H., and McMurry, P. H.: Variability in morphology, hygroscopicity, and optical properties of soot aerosols during atmospheric processing, *Proc. Natl. Acad. Sci.* USA, 105, 10291-10296, 2008.

Zhang, S. L., Ma, N., Kecorius, S., Wang, P. C., Hu, M., Wang, Z. B., Größ, J., Wu, Z. J., and Wiedensohler, A.: Mixing state of atmospheric particles over the North China Plain, *Atmos. Environ.*, 125, Part A, 152-164, 2016a.

Zhang, Y., Zhang, Q., Cheng, Y., Su, H., Kecorius, S., Wang, Z., Wu, Z., Hu, M., Zhu, T., Wiedensohler, A., and He, K.: Measuring the morphology and density of internally mixed black carbon with SP2 and VTDMA: new insight into the absorption enhancement of black carbon in the atmosphere, *Atmos. Meas. Tech.*, 9, 1833-1843, 2016b.

Zheng, G. J., Duan, F. K., Su, H., Ma, Y. L., Cheng, Y., Zheng, B., Zhang, Q., Huang, T., Kimoto, T., Chang, D., Pöschl, U., Cheng, Y. F., and He, K. B.: Exploring the severe winter haze in Beijing: the impact of synoptic weather, regional transport and heterogeneous reactions, *Atmos. Chem. Phys.*, 15, 2969-2983, 2015.

Atmos. Chem. Phys. Discuss., doi:10.5194/acp-2017-222, 2017
Manuscript under review for journal Atmos. Chem. Phys.
Discussion started: 19 April 2017

Atmospheric Chemistry and Physics Discussions

Table 1. Comparison of BC mixing state measured in our study and previous studies.

Site	Air mass type	D_p (nm)	D_c (nm)	*CT* (nm)	Reference
Xianghe, China	Polluted regional air	200-350	~80-200	~50-150	This study
Fukue Island, Japan	Asian outflow	~320	~200	~60	Shiraiwa et al., 2008
Long Island, USA	Suburban air	~150-180	~80	~20-50	Sedlacek et al., 2012
Paris, France	Urban air	~265	~200	~33	Laborde et al., 2013
Pasadena, USA	Urban air	~170-260	135-200	~22	Taylor et al., 2015
Toronto, Canada	Urban air	~200	~180	~10	Lee et al., 2015

Atmos. Chem. Phys. Discuss., doi:10.5194/acp-2017-222, 2017
Manuscript under review for journal Atmos. Chem. Phys.
Discussion started: 19 April 2017

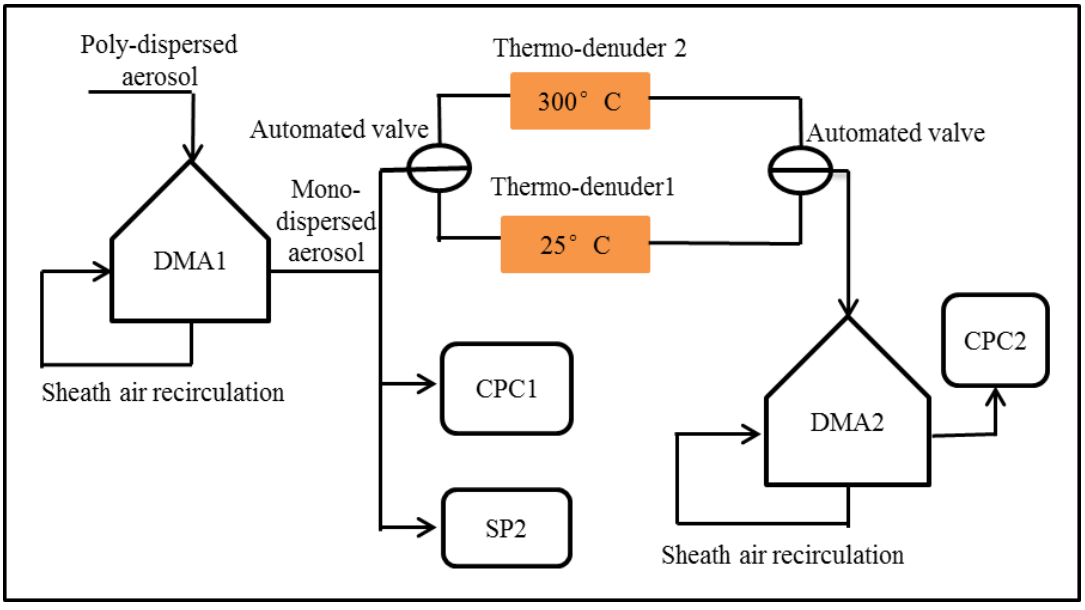

Figure 1. Schematic of instrument setup.

Atmos. Chem. Phys. Discuss., doi:10.5194/acp-2017-222, 2017
Manuscript under review for journal Atmos. Chem. Phys.
Discussion started: 19 April 2017

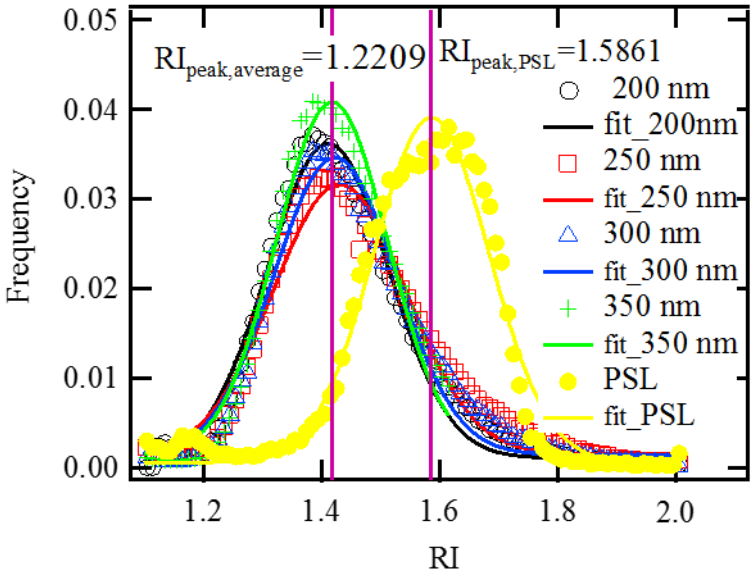

Figure 2. The distribution of RI for size-resolved non-BC particles and PSL sphere.

Atmos. Chem. Phys. Discuss., doi:10.5194/acp-2017-222, 2017
Manuscript under review for journal Atmos. Chem. Phys.
Discussion started: 19 April 2017

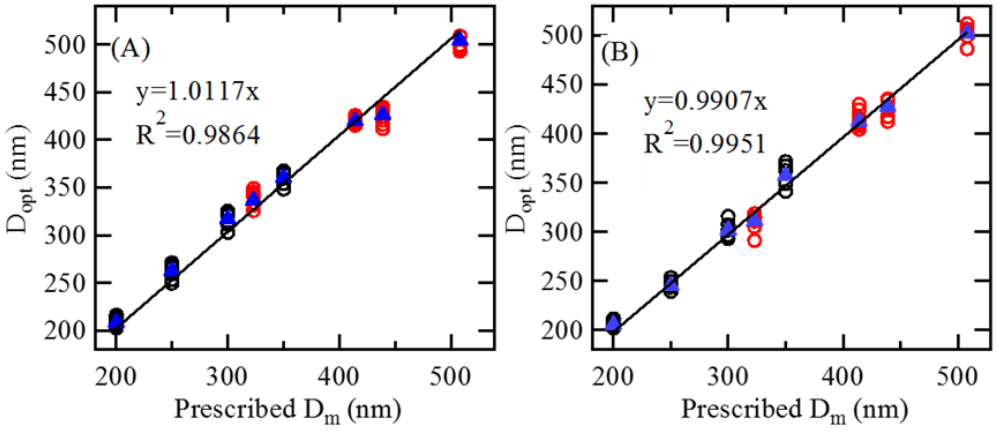

Figure 3. Comparison the prescribed mobility size (D_m) by DMA1 and the optical size (D_{opt}) determined by SP2 for (A) non-BC particles and (B) internally-mixed BC particles. The solid lines are fitted based on average data (blue triangle); the black circles and red circles represent the singly charged particle samples and doubly/ multiply charged particle samples, respectively.

Atmos. Chem. Phys. Discuss., doi:10.5194/acp-2017-222, 2017
Manuscript under review for journal Atmos. Chem. Phys.
Discussion started: 19 April 2017

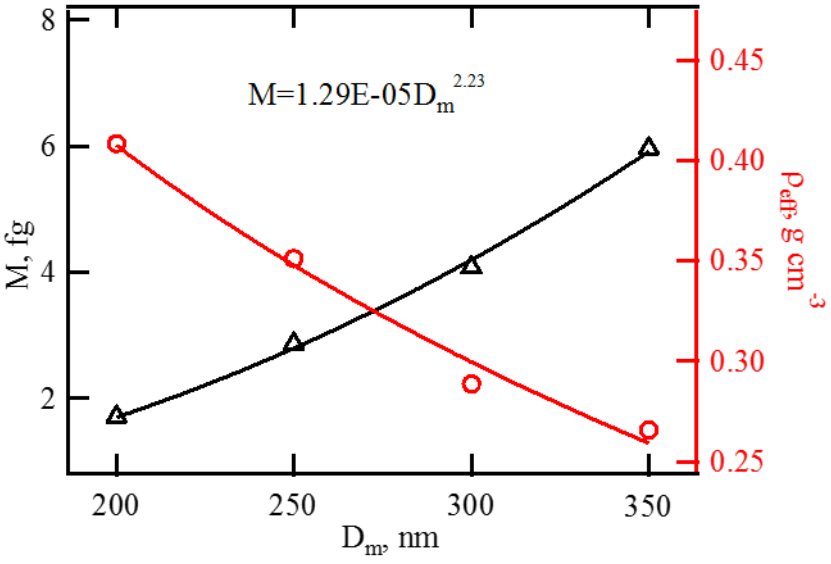

Figure 4. Mass (M) and effective density (ρ_{eff}) of externally-mixed BC at different mobility diameters (D_m).

Atmos. Chem. Phys. Discuss., doi:10.5194/acp-2017-222, 2017
Manuscript under review for journal Atmos. Chem. Phys.
Discussion started: 19 April 2017

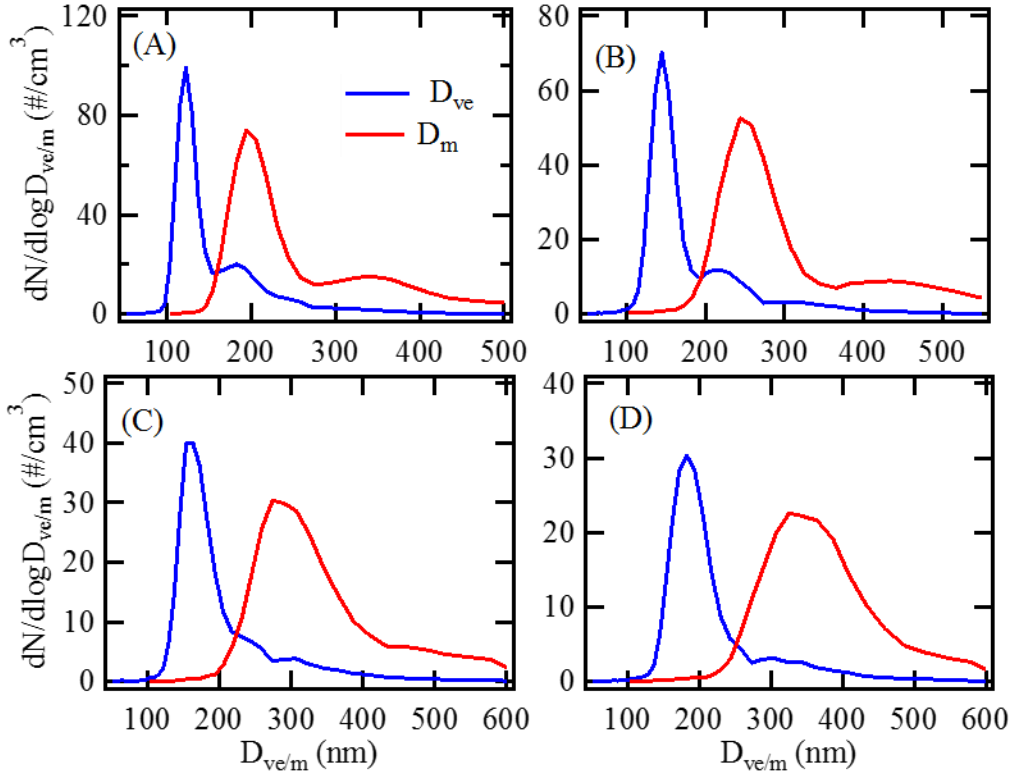

Figure 5. The volume equivalent diameter (D_{ve}) and mobility diameter (D_m) distribution for size-resolved externally-mixed BC at (A) 200 nm , (B) 250 nm (B), (C) 300 nm and (D) 350 nm.

Atmos. Chem. Phys. Discuss., doi:10.5194/acp-2017-222, 2017
Manuscript under review for journal Atmos. Chem. Phys.
Discussion started: 19 April 2017

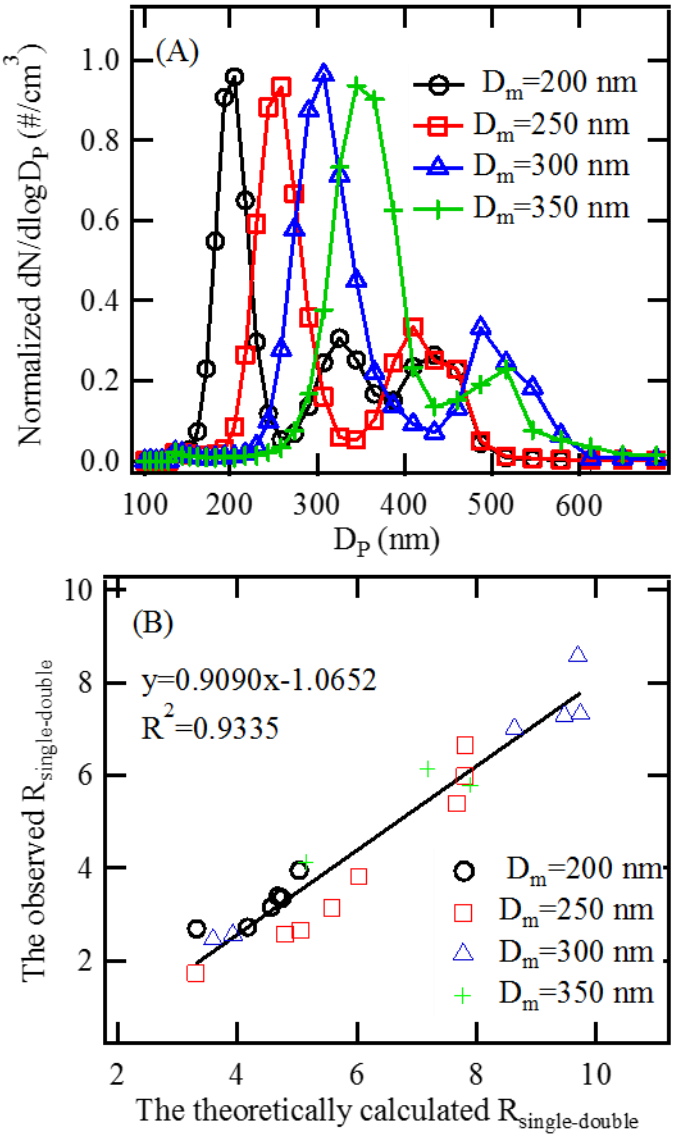

Figure 6. (A) Normalized size distribution of size-resolved aerosol particles (including non-BC particles, internally-mixed BC and externally-mixed BC) at 200-350 nm derived from SP2 measurement; (B) comparison of the observed ratio of singly charged particles and doubly charged particles from the SP2 measurement (i.e., the observed $R_{single\text{-}double}$) and that from theoretical calculation(i.e., the theoretically calculated $R_{single\text{-}double}$).

Atmos. Chem. Phys. Discuss., doi:10.5194/acp-2017-222, 2017
Manuscript under review for journal Atmos. Chem. Phys.
Discussion started: 19 April 2017

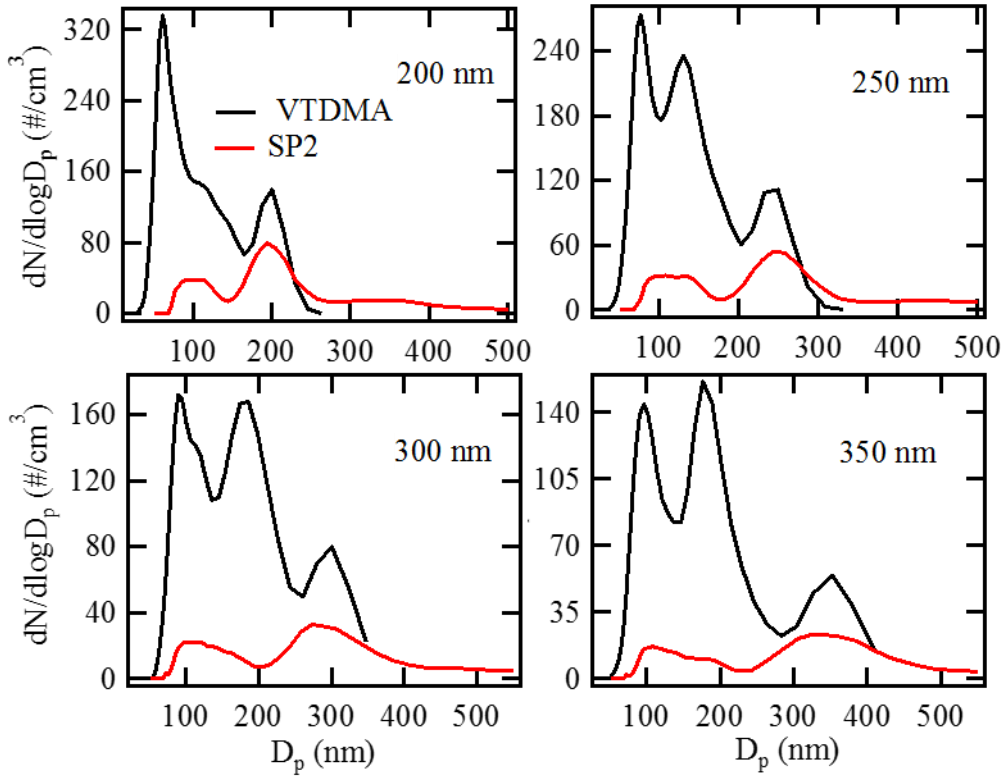

Figure 7. Size distributions of rBC (externally-mixed BC and BC core of internally-mixed BC) measured by SP2 (red lines) and that of residual materials from our VTDMA measurement at 300 ℃ (black lines). Before the measurements were taken with SP2 and VTDMA at 300 ℃, the initial particle sizes selected by DMA1 were 200, 250, 300 and 350 nm.

Atmos. Chem. Phys. Discuss., doi:10.5194/acp-2017-222, 2017
Manuscript under review for journal Atmos. Chem. Phys.
Discussion started: 19 April 2017

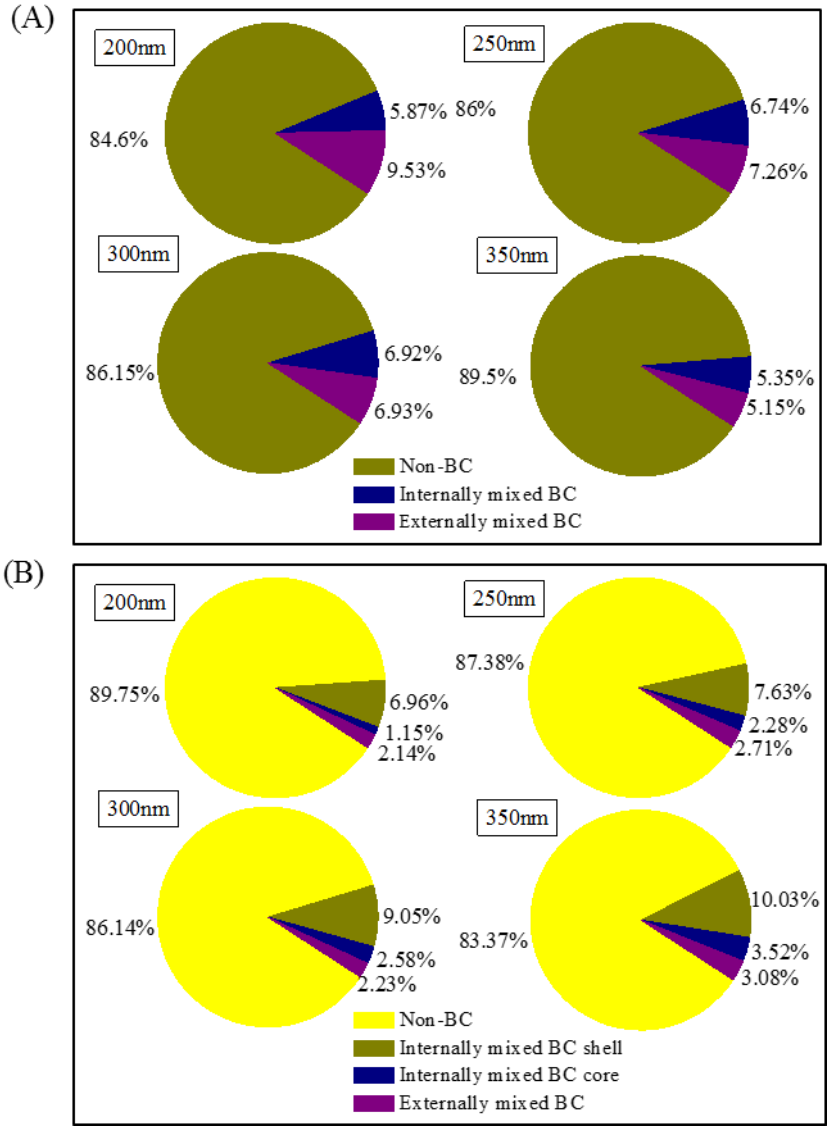

Figure 8. (A) The number and (B) mass composition of ambient particle samples with different mobility diameters (200, 250, 300 and 350 nm) selected by DMA1.

Atmos. Chem. Phys. Discuss., doi:10.5194/acp-2017-222, 2017
Manuscript under review for journal Atmos. Chem. Phys.
Discussion started: 19 April 2017

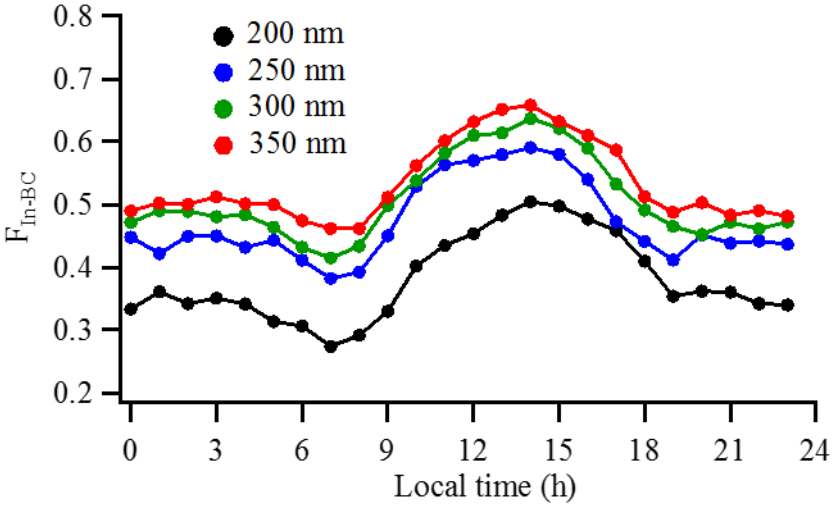

Figure 9. Diurnal variation of the fraction of internally-mixed BC particles (F_{in}) with different mobility diameters (200, 250, 300 and 350 nm) selected by DMA1.

Atmos. Chem. Phys. Discuss., doi:10.5194/acp-2017-222, 2017
Manuscript under review for journal Atmos. Chem. Phys.
Discussion started: 19 April 2017

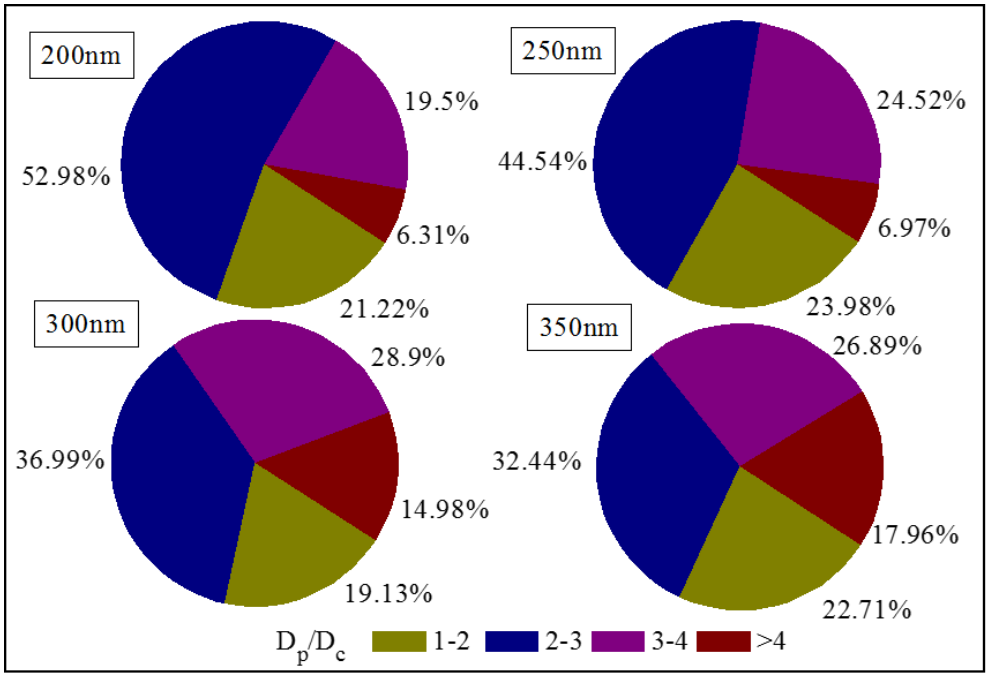

Figure 10. The number fraction of different mixing state for internally-mixed BC particles with DMA1 selecting size (200-350 nm).

Atmos. Chem. Phys. Discuss., doi:10.5194/acp-2017-222, 2017
Manuscript under review for journal Atmos. Chem. Phys.
Discussion started: 19 April 2017

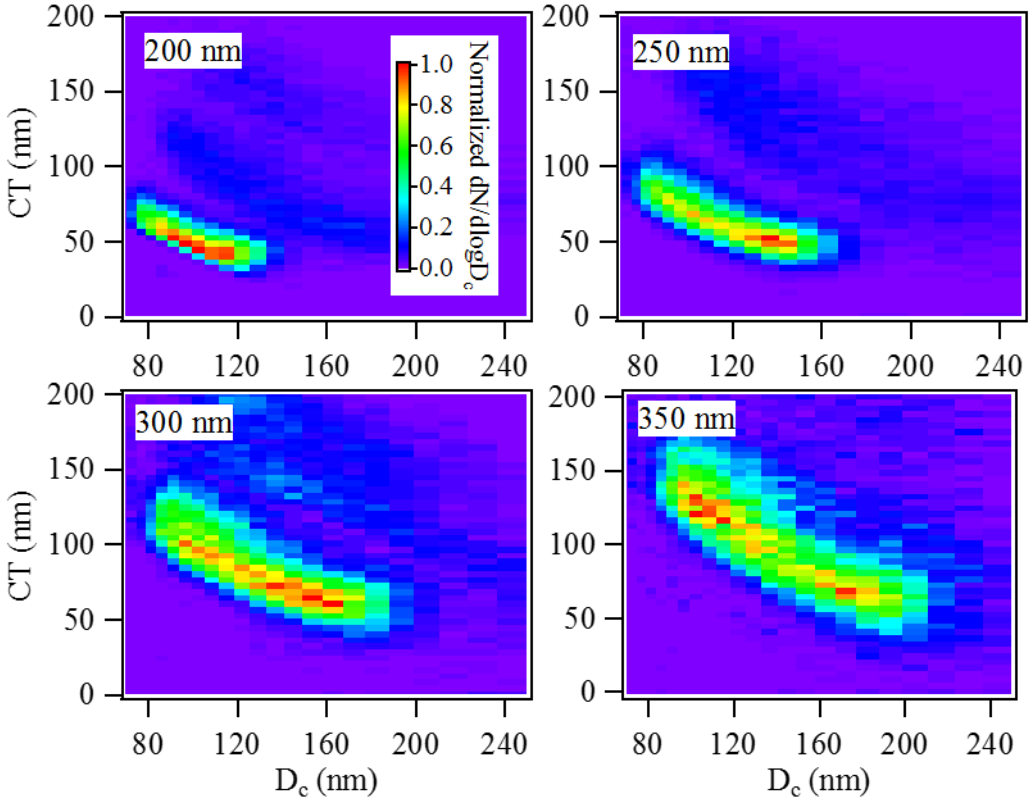

Figure 11. Coating thickness (*CT*) of internally-mixed BC particles at 200-350 nm (selected by DMA1) as a function of rBC core size (D_c).